


1 The case of a southern European glacier  that survived
2 Roman and Medieval warm periods but is disappearing
3 under recent warming

4 Ana Moreno¹, Miguel Bartolomé², Juan Ignacio López-Moreno¹, Jorge Pey^{1,3}, Juan
5 Pablo Corella⁴, Jordi García-Orellana^{5,6}, Carlos Sancho[‡], María Leunda^{7,8}, Graciela Gil-
6 Romera^{9,1}, Penélope González-Sampériz¹, Carlos Pérez-Mejías¹⁰, Francisco Navarro¹¹,
7 Jaime Otero-García¹¹, Javier Lapazaran¹¹, Esteban Alonso-González¹, Cristina Cid¹²,
8 Jerónimo López-Martínez¹³, Belén Oliva-Urcia¹³, Sérgio Henrique Faria^{14,15}, María José
9 Sierra⁴, Rocío Millán⁴, Xavier Querol¹⁶, Andrés Alastuey¹⁶ and José M. García-Ruiz¹

1. Departamento de Procesos Geoambientales y Cambio Global, Instituto Pirenaico de Ecología – CSIC, Zaragoza, Spain
2. Departamento de Geología, Museo de Ciencias Naturales - CSIC, Madrid, Spain
3. Fundación Aragonesa para la Investigación y el Desarrollo, ARAID, Zaragoza, Spain
4. CIEMAT — Environmental Department (DMA), Avenida Complutense 40, Madrid, Spain
5. Institut de Ciència i Tecnologia Ambientals, Universitat Autònoma de Barcelona, Barcelona, Spain
6. Departament de Física, Universitat Autònoma de Barcelona, Barcelona, Spain
7. Institute of Plant Sciences & Oeschger Centre for Climate Change Research, Bern, Switzerland
8. Swiss Federal Research Institute for Forest, Snow and Landscape Research WSL, Birmensdorf, Switzerland
9. Department of Ecology, Faculty of Biology, Philipps-Marburg University, Marburg, Germany
10. Institute of Global Environmental Change, Xi'an Jiaotong University, Xi'an, China
11. Departamento de Matemática Aplicada a las TIC, ETSI de Telecomunicación, Universidad Politécnica de Madrid, Madrid, Spain
12. Centro de Astrobiología – CSIC-INTA, Madrid, Spain
13. Departamento de Geología y Geoquímica, Facultad de Ciencias, Universidad Autónoma de Madrid, Madrid, Spain
14. Basque Centre for Climate Change (BC3), Leioa, Spain
15. IKERBASQUE, Basque Foundation for Science, Bilbao, Spain
16. Institute of Environmental Assessment and Water Research – CSIC, Barcelona, Spain

‡ Deceased

Corresponding author: Ana Moreno (amoreno@ipe.csic.es) ORCID: 0000-0001-7357-584X

Keywords

Pyrenees, mountain glacier, current global warming, Medieval Climate Anomaly, Monte Perdido

37 Abstract

38 Mountain glaciers have generally experienced an accelerated retreat over the last
39 three decades as a rapid response to current global warming. However, the response
40 to previous warm periods in the Holocene is not well-described for glaciers of the
41 southern Europe mountain ranges, such as the Pyrenees. The situation during the
42 Medieval Climate Anomaly (900-1300 CE) is particularly relevant since it is not certain
43 whether the southern European glaciers just experienced significant ice loss or
44 whether they actually disappeared. We present here the first chronological study of a
45 glacier located in the Central Pyrenees (NE Spain), the Monte Perdido Glacier (MPG),
46 carried out by different radiochronological techniques and a comparison with
47 geochemical proxies from neighboring paleoclimate records. The chronological model
48 evidences that the glacier endured during the Roman Period and the Medieval Climate
49 Anomaly. The lack of ice record dated from the last 600 years suggests that the ice
50 formed during the Little Ice Age has melted away. The analyses of several metals with
51 anthropogenic source that characterize the Industrial Period, such as Zn, Se, Cd, Hg
52 and Pb, reveal low concentrations in MPG ice, which provides further evidence about
53 the absence of the most recent ice. This study confirms the exceptional warming of the
54 last decades in the context of the last two millennia.


55

56 1. Introduction

57 Mountain glaciers are sensitive to climate variations on temporal scales from decades
58 to centuries. It is well known that summer temperature and winter precipitation are
59 the most important climate parameters influencing glacier mass balance (Oerlemans,
60 2001). Therefore, continuous records of past glacier size fluctuations provide valuable
61 information about the timing and magnitude of Holocene climate shifts, which
62 contributed to explain the characteristics and evolution of plant cover, human
63 movements and land use (Solomina et al., 2015, 2016). Several glacier advances during
64 the Neoglacial (which started around 6000-5000 years ago) have been identified and
65 associated to sustained cooling periods across the North Atlantic (Wanner et al., 2011).
66 The most recent period of global glacier expansion took place during the Little Ice Age
67 (LIA), beginning in the 13th century and reaching a maximum between the 17th and 19th
68 centuries (Solomina et al., 2016). Afterwards, most glaciers worldwide have retreated
69 rapidly, as indicated by measurements of ice volume and ice-covered area, and this
70 trend seems to have accelerated over the last three decades (Marzeion et al., 2014;
71 Zemp et al., 2015, 2019).

72 Despite broad agreement on millennial-scale trends in global glacier fluctuations and
73 Holocene climate variability (Davis et al., 2009; Solomina et al., 2015), regional
74 variations are not so well constrained. The Pyrenees is a mountain range that currently
75 hosts the majority of the southernmost glaciers in Europe. In this mountain chain there
76 is a significant lack of knowledge about Holocene glacier fluctuations, with few
77 evidences of Neoglacial advances (García-Ruiz et al., 2020). Based on Pyrenean tree-
78 ring chronologies, summer temperatures during the Medieval Climate Anomaly (MCA,
79 circa 900–1300 CE) were estimated to have been as warm as those of the 20th century
80 (Büntgen et al., 2017), but no information is available on the glacier response to MCA
81 warming. Conversely, glacier advance during the LIA is well constrained in the
82 Pyrenees (García-Ruiz et al., 2014; González Trueba et al., 2008; Hughes, 2018; Oliva et
83 al., 2018) and a significant deglaciation is also evident in recent times (López-Moreno
84 et al., 2016; Rico et al., 2017). In particular, the period from the 1980s to present has
85 been the most intense in terms of the number of glaciers that disappeared (from 39
86 inventoried Pyrenean glaciers in 1984 to 19 at present; Rico et al. 2017). Given the

small size of the Pyrenean glaciers and their current critical situation in the context of global warming, we hypothesize that they could have disappeared completely during warm periods such as the MCA.

This study is focused on Monte Perdido Glacier (MPG), located in the Marboré Cirque in the Spanish Central Pyrenees. MPG is currently one of the  best monitored small glaciers (<0.5 km²) worldwide (López-Moreno et al., 2016, 2019). Previous research based on different ground-based remote sensing techniques has demonstrated a rapid retreat of this glacier, with an average loss of ice thickness of about one meter per year since 1981 (López-Moreno et al., 2016, 2019). This glacier is located in one of the few valleys in the Pyrenees where information about Holocene glacier fluctuations exists. The outermost moraine in Marboré Cirque was recently dated at 6900 ± 800 ³⁶Cl yr BP (García-Ruiz et al., 2020), which is the oldest Holocene date available for glacial deposits in Spain, and indicates a glacier advance during the Neoglacial period. Other minor advances would have occurred in MPG prior to the LIA, as inferred from three polished surfaces dated at 3500 ± 400, 2500 ± 300 and 1100 ± 100 ³⁶Cl yr BP (García-Ruiz et al., 2020). Unfortunately, no information has been obtained on the glacier response to Roman or MCA warming periods, remaining an open question whether MPG just experienced significant ice loss or melted away totally. Most likely, the voluminous moraine at the foot of the Monte Perdido Massif was deposited during the LIA, indicating an important glacier advance. These results, together with the evidences of long-term retreat from its LIA position indicated by pictures and moraines, suggested that this glacier could disappear over the next few decades (López-Moreno et al., 2016).

The present study aims to reconstruct the chronology of MPG ice sequence by using a variety of dating techniques and the analysis of several proxies associated to environmental and anthropogenic changes measured on a set of samples taken from a transect. Such analyses will fill the existing knowledge gaps and answer the key question of whether Pyrenean glaciers may have survived previous Holocene warm periods.

2. Study area

The MPG (42°40'50"N; 0°02'15"E) is located in the Central Spanish Pyrenees, in the Ordesa and Monte Perdido National Park (OMPNP) (Fig. 1). It currently consists of two separate ice bodies, which were connected in the past. Both are north facing, lie on structural flats beneath the main summit of the Monte Perdido Peak (3355 m a.s.l.) and are surrounded by vertical cliffs of 500–800 m in height. At the base of the cliffs, the Cinca River flows directly from the glacier and the surrounding slopes, and has created a longitudinal west–east basin called the Marboré Cirque (5.8 km²). This is the area within the Pyrenees with the highest variety of recent morainic deposits (García-Ruiz et al., 2014, 2020). Additionally, a 6 m thick sediment core obtained in 2011 from a lake inside the cirque (Marboré Lake) provided valuable information from the last 14,600 years of the depositional evolution of the lake (Oliva-Urcia et al., 2018) and of the regional variations in vegetation cover (Leunda et al., 2017). The Marboré Lake (2595 m a.s.l.) is located in the Marboré or Tucarroya Cirque, in the northern face of the Monte Perdido massif. The distance between the lake and the MPG is approximately 1300 m and, therefore, both have been affected by similar palaeoenvironmental conditions.

The total surface area of MPG in 2016 was 0.385 km², with an average decrease in glacier ice thickness of 6.1 m during the period 2011 - 2017 (López-Moreno et al., 2019). According to recent measurements of air temperature (July 2014 to October 2017), the 0 °C isotherm lies at 2945 m a.s.l., suggesting that the potential glacier accumulation area is very small, even inexistent during warm years. The average summer (June to September) temperature at the foot of the glacier from 2014 to 2017 has been of 7.3 °C (López-Moreno et al., 2019). No direct observations of precipitation are available at the glacier location, but the maximum accumulated snow by late April in the three available years (2014, 2015 and 2017, when no scanning limitations occurred and the whole glacier was scanned) was 3.23 m, and field-measured average snow density was 454 kg m⁻³, indicating that total water equivalent during the main accumulation period (October to April) could be equivalent to about 1500 mm (López-Moreno et al., 2019).

3. Material and methods

147 3.1. Ice sampling and storage

148 Ice sampling on MPG was carried out in September 2017 along a chrono-stratigraphical
149 sequence covering from the ~~oldest to the newest~~ ice preserved in the glacier, following
150 the isochronal layers that emerge in the ablation zone (Fig. 2A). Unfortunately, the
151 extraction of vertical cores was not possible because the glacier does not currently
152 meet any of the usual glacio-meteorological and topographical criteria required to
153 obtain a preserved ice-core stratigraphy. The unfulfilled criteria include low
154 temperatures to prevent water percolation or a large extension and flat surface
155 topography to minimize the influence of glacier flow (Garzonio et al., 2018). Samples
156 were collected in an area with no evidence of current ice movement ^{major} ~~(or very low)~~, as
157 confirmed by results from interferometric radar and GNSS measurements (López-
158 Moreno et al., 2019). Due to the small size of this glacier, we expected the ice to be
159 frozen ^{the permafrost} to bedrock, and hence nearly stagnant, ^{thereby reaching a} ~~to become of~~ substantial age, as
160 indicated by previous studies in similar glaciers (Gabrielli et al., 2016; Haeberli et al.,
161 2004). The sampling sector lies in the ablation zone of MPG and has been eroded to
162 form a current steady slope of 20° where it is possible to observe the primary
163 stratigraphy, marked by clear debris-rich layers. The distribution of these debris-rich
164 layers is rather regular and extends laterally (Fig. 2B), as would be expected for the
165 primary stratification resulting from the original deposition at ^{the} surface of snow and
166 debris. Therefore, these layers are considered isochrones, and confirm and facilitate
167 the sampling along the slope, from the oldest to the ^{youngest} ~~newest~~ ice ^{preserved in the}
168 glacier.

169 We measured one-meter thickness using a Jacob's staff at each sampling point along
170 the slope (Fig. 2B). The tilt of the ice layers was unclear but, since previous studies
171 calculated about 30 m of ice thickness (López-Moreno et al., 2019), the ice layers are
172 probably quite tilted downward as detailed in ^{Fig. 2A}. Once cleaned the most
173 superficial ice (ca. 50 cm) to avoid possible ice formed recently, we recovered at every
174 sampling position 3–4 small horizontal cores (6 cm in diameter and 25 cm in length)
175 using a custom stainless-steel crown adaptor on a cordless power drill (Fig. 2C).
176 Following this sampling procedure we recovered a total of 100 samples. The ice
177 samples were stored in a freezer room at the IPE-CSIC in Zaragoza until they were

178 melted and analysed to obtain their chronology combining ^{210}Pb , ^{137}Cs and ^{14}C
179 techniques, and their geochemical composition in trace metals, such as Pb or Hg (see
180 below).

181 3.2. Dating by ^{210}Pb and ^{137}Cs .

182 The isotope ^{137}Cs , usually associated to the fallout from nuclear tests during the 1950s
183 and the 1960s, as well as the Chernobyl (1986) and Fukushima (2011) accidents, was
184 investigated by γ -spectrometry in five samples recovered towards the top of the MPG
185 chronological sequence (MP-61, MP-82, MP-97, MP-98, MP-100, Table 1). In addition,
186 ten samples were selected to perform a ^{210}Pb analysis as an independent dating
187 method to obtain the age model of approximately the last hundred years of glacier ice
188 (Eichler et al., 2000; Herren et al., 2013). These samples were selected also from the
189 top of the ice sequence to collect the younger ice (Table 2). Determination of ^{210}Pb
190 activities was accomplished through the measurement of its daughter nuclide, ^{210}Po ,
191 by α -spectrometry following the methodology described in (Sanchez-Cabeza et al.,
192 1998) (Table 2).

193 3.3. Dating by ^{14}C method.

194 Sixteen accelerator mass spectrometry (AMS) ^{14}C dates from MPG ice were obtained
195 by combining bulk organic matter (9 samples), pollen concentrates (3 samples), bulk
196 sediment accumulated in filters (2 filters), and water-insoluble organic carbon (WIOC)
197 particles (2 samples) (Table 3). The procedure to select these samples was as follows:

198 (i) Using a binocular microscope [x10], we picked up organic particles for dating from
199 selected ice samples. However, the small size of the handpicked organic remains
200 prevented us from classifying them. As a result, we obtained 9 samples (MP-1, MP-42,
201 MP-48, MP-67, MP-68, MP-69, MP-70, MP-73, MP-100, Table 3) that were sent to the
202 Direct AMS laboratory (Seattle, USA) for dating. The selection of those nine samples
203 was based on the amount of debris found in the sample, once the ice was melted

204 (ii) Pollen concentrates were prepared from three samples (MP-30, MP-70 and MP-
205 100) to complete the previous set with the aim of replicating some of the results (MP-
206 70 and MP-100) and obtaining new dates (MP-30). Preparation followed the standard

207 palynological method, including a chemical treatment and mineral separation in heavy
208 liquid (Thoulet: density 2.0; Moore et al., 1991). The effects of meltwater percolation
209 on pollen in snow, firn and glacial ice are not fully understood and currently challenge
210 the use of pollen in ice-core studies (Ewing et al., 2014). Just in few cases pollen has
211 appeared as a potential dating material, when seasonal layers are preserved (Festi et
212 al., 2017). Yet, pollen concentrates have been used in other type of archives with high
213 success (Fletcher et al., 2017), opening the door to apply the same methodology here.

214 (iii) Two ice samples (MP-67 and MP-81), which appeared darker than others once
215 melted, were filtered throughout a filtration line connected to a vacuum pump using
216 47 mm quartz fiber filters (PALL tissuquartz 2500QAT-UP), parameterized at controlled
217 conditions (temperature: 22 – 24 °C; relative humidity 25 – 35 %) and weighted twice
218 in different days. Abundant material was obtained, but no control was made on the
219 composition and amount of organic material versus other types of input. The three
220 concentrated pollen samples and the two filters were dated at the same ¹⁴C dating
221 laboratory (Direct AMS, Seattle, USA) (Table 3).

222 (iv) Finally, two more samples were dated at the Laboratory of Environmental
223 Chemistry, Paul Scherrer Institute (Switzerland) removing the outer part of the ice core
224 segment for decontamination purposes (Jenk et al., 2009). Since organic fragments
225 (plants, wood, insects) are rarely found in mountain glaciers, a new, complementary
226 dating tool was recently developed based on extracting the microgram-amounts of the
227 water-insoluble organic carbon (WIOC) fraction of carbonaceous aerosols embedded in
228 the ice matrix for subsequent ¹⁴C dating (Uglietti et al., 2016). These two samples,
229 labelled as MP10m and MP59m at the WIOC facility (Table 3), were selected as the
230 only ones with sufficient ice volume available.

231 Once the 16 radiocarbon ages were obtained, we converted them into calendar ages
232 by using the CALIB 5.0.2 software, which uses the most updated dataset, INTCAL13
233 (Reimer et al., 2013) (Table 3). The median of the one-σ probability interval was
234 selected for these dates, resulting in highly variable errors in the calendar ages
235 obtained (from 30 years on the bulk organic samples to more than 200 years on pollen
236 and WIOC samples). While the first method to select organic remains at the

237 microscope resulted the best option, the pollen concentration and filtering methods
238 used to isolate organic matter to be dated by ^{14}C were, unfortunately, not successful.
239 Finally, from the initial 16 dates, we had to discard seven according to the following
240 criteria (see the “comments” column in Table 3):

- 241 - Sample MP-46 (D-AMS 025295) was the only one discarded from the nine initial
242 bulk organic matter samples. We suspect that the very recent age obtained
243 (1897 ± 20 CE, Table 3) is due to the sample contamination, since small plastic
244 debris coming off from the painting used in the coring device were identified
245 under the microscope.
- 246 - From the two WIOC-dated samples, one was discarded (MP10m) due to the
247 low carbon content ($5.3 \mu\text{g}$), thus providing too inaccurate results (854 ± 721
248 CE, with an unacceptable large uncertainty). The other sample (MP59m), with
249 higher organic carbon content ($28.7 \mu\text{g}$), was incorporated into the age model
250 in spite of its error above 200 yr (1046 ± 242 CE).
- 251 - The three pollen concentrates provided unreliably old dates with very high
252 errors, likely due to the small amount of pollen that we were able to
253 concentrate (errors above 200 yr, Table 3). Obtaining old dates from pollen is a
254 quite common problem not yet solved in the literature (Kilian et al., 2002).
- 255 - Similarly, we discarded the two filter samples MP-67 and MP-81 (D-AMS
256 029894 and D-AMS 033972, respectively). The material accumulated in the
257 filters was a mixture of particles containing detrital carbonate eroded from
258 Eocene limestones or supplied by Saharan dust, which was not removed and
259 probably influenced the results incorporating allochthonous carbon to the
260 samples.

261 Finally, nine dates were employed to infer the chronology of the MPG sequence. The
262 depth–age model was created using a linear regression in the R package CLAM 2.2
263 (Blaauw, 2010; Blaauw et al., 2019).

264 *3.4. Trace elements in soluble and insoluble material.*

265 35 selected ice samples from the altitudinal transect were melted and filtered through
266 a filtration ramp connected to a vacuum pump using 47 mm quartz fibre filters (PALL

tissuquarzt 2500QAT-UP). Filters were pre-heated at 250 °C and thereafter prepared in controlled conditions (temperature: 22 – 24 °C; relative humidity: 25 – 35 %) before and after filtration. Subsequently, they were weighted in two different days. Mass difference between blank and sampled filters was used to calculate the amount of insoluble material entrapped in ice samples. For every sample, an aliquot and a filter were obtained. From aliquots, anions and cations, as well as major and trace elements were determined. From filters, we determined major and trace elements, as well as organic and elemental carbon, following the method devised by Pey et al. (2013) (Table 4). Basically, an acidic digestion (HNO₃:HF:HClO₄) of half of each filter was conducted, driven to complete dryness, being the remaining material re-dissolved in HNO₃. Inductively coupled plasma mass spectrometry (ICP-MS) and inductively coupled plasma atomic emission spectroscopy (ICP-AES) were used to determine major and trace elements, respectively. From the other half of each filter, a 1.5 cm² section was used to determine Organic Carbon (OC) and Elemental Carbon (EC) concentrations by using a SUNSET thermo-optical analyzer, following the EUSAAR_2 temperature protocol. Table 1 also contains the Enrichment Factors (EFs), calculated as follows:

$$EF_{iCodd} = \frac{X_{iCodd}/Al_{Codd}}{X_{iUC}/Al_{UC}} \quad EF_{iMPGID} = \frac{X_{iMPGID}/Al_{MPGID}}{X_{iUC}/Al_{UC}} \quad EF_i = \frac{X_{iCodd}/Al_{Codd}}{X_{iMPGID}/Al_{MPGID}}$$

where EF_{iCodd} is the Al-normalised Enrichment Factor with respect to the Upper Crust (UC, Taylor and McLennan (1995)) of an 'i' element in the current Ordesa's deposited dust (Codd); EF_{iMPGID} is the Al-normalised Enrichment Factor with respect to the UC of an 'i' element in the current MPG ice dust (MPGID); and EF_i is the Al-normalised Enrichment Factor with respect to Codd of an 'i' element in the MPGID.

Regarding the Pb/Al ratio, we carried out a normalization with Al in both, ice and lake records, to disentangle the anthropogenic lead variability from possible detrital inputs. Aluminium has been selected for normalization since this lithogenic element is immobile and abundant in carbonated watersheds (Corella et al., 2018).

3.5. Hg determination.

294 Total Hg concentration measurements were carried out in 21 selected samples by
295 Atomic Absorption Spectrophotometry using an Advance Mercury Analyzer (AMA 254,
296 LECO Company). This equipment is specifically designed for direct mercury
297 determination in solid and liquid samples without sample chemical pre-treatment.
298 Certified reference materials were used to determine the accuracy and precision of the
299 Hg measurements. These reference materials were ZC73027 (rice, $4.8 \pm 0.8 \mu\text{g kg}^{-1}$)
300 and CRM051–050 (clay soil, $4.08 \pm 0.09 \text{ mg kg}^{-1}$). The standard deviation (repeatability)
301 was $\leq 15 \%$ and the relative uncertainty associated with the method (with a confidence
302 level of about 95 %) was $\pm 20 \%$. All analyses were run at least three times. Total metal
303 concentrations were expressed in $\mu\text{g g}^{-1}$ of dry weight sediment due to the low
304 amount detected.

305 4. Results

306 4.1. Chronological model

307 To date the ice sequence from MPG we compiled the results from ^{137}Cs , ^{210}Pb and ^{14}C
308 methods. First, ~~it is remarkable~~ the absence of ^{137}Cs in the five samples analyzed (Table
309 1). This implies that all samples are older than 60–65 years and therefore they were
310 not exposed to the atmosphere after 1950 CE. Another possibility that was discarded
311 upon obtaining ^{14}C dates, is that all samples were younger than 1950 CE. Similarly,
312 ^{210}Pb activity was also undetectable in most cases, except in three samples (MP-100,
313 MP-73 and MP-76) with concentrations above minimum detection activity (MDA; Table
314 2). These three samples contained a large amount of lithogenic particulate material
315 from atmospheric dust or ash deposits, likely causing the observed values. Thus, the
316 absence of ^{210}Pb activity in the analysed samples suggests that MPG ice samples were
317 very likely older than 100 years and the ^{210}Pb had completely decayed. We then built
318 up the proposed MPG chronology using only AMS ^{14}C dating.

319 Regarding ^{14}C dating, we took most of the ice samples for dating in sections where
320 dark debris layers alternated every ca. 5 m with cleaner and clearer ice (Fig. 2). The
321 debris-rich layers were composed of detrital, silty-sandy size deposits, likely coming
322 from wind-blown particles (e.g. black carbon-rich particles, dust) and from erosive
323 processes of the limestone catchment, including the fall of gravel-sized particles from

the surrounding cliffs. These debris-rich layers do not have a subglacially derived origin since they are observed all along the sample profile and large accumulation of debris or pinnacles, both characteristics of subglacially derived glacier till, were not found in MPG. These debris layers contain more organic remains than those formed by clear ice, making them ideal spots to find datable remains.

Interestingly, the frequency of debris layers increases towards the top of the glacier sequence. We consider the accumulation of debris layers to be indicative of reduced ice accumulation and dominance of ablation periods. In such situations, the detrital and organic material concentrates as the ice melts, giving its characteristic dark colour to the ice layers. The major concentration of such layers occurred among samples MP-67 and MP-73 (Table 3), thus suggesting the dominance of ablation processes. Therefore, we run the depth–age model setting a hiatus at 73 m depth, where we think an interruption in the ice accumulation was produced. Finally, as explained in the methods section, the age-model was constructed with 9 of the initially dated 16 samples (Table 3). Given the scattered depths at which dates concentrate, we chose to perform a non-smooth, linear regression for preventing any model over-fitting and a spurious age–depth relationship (Fig. 3). Full details on how the model was performed and a reproducible workflow with the current chronological dataset are stored at <https://zenodo.org/record/3886911>.

4.2. Trace elements

We have used the averaged concentration values of major and trace elements currently obtained at a monitoring station located at OMPNP (8 km away from the MPG, at 1190 m a.s.l.), where deposited atmospheric particulate matter is sampled monthly (Table 4) (Pey et al., 2020). Interestingly, the elements that are abundant nowadays in the Ordesa station are not so frequent in the ice from MPG. Indicators such as organic carbon, Zn, Se and Cd concentrations, all of which are potential proxies of current anthropogenic emissions, are much higher in the samples from Ordesa, which are representative of today's atmosphere, than in the ice samples from the MPG. The low concentration of these elements in MPG samples could indicate their disappearance from glacier surface layers due to its continuous melting. This supports

our suggested age model (Fig. 3), in which ages from the Industrial Period are not recorded. Conversely, the Al-normalised enrichment factor (EF) of Ti, Mn, Cr, Co, Ni, Cu and Pb, elements linked to the natural fraction (dust deposition, lithogenic elements) and mining activities (Corella et al., 2018), are more abundant in the MPG ice samples than in the present-day Ordesa aerosols (Table 4). From them, Cu and Pb were markedly enriched (by a factor >6) in the MPG ice samples compared with the current deposited aerosols in Ordesa station.

5. Discussion


5.1. Dating Monte Perdido Glacier ice sequence

Dating the ice from non-polar glaciers is challenging and often problematic as annual layer counting is precluded due to periods without net accumulation, and to common ice deformation caused by glacier flow (Bohleber, 2019; Festi et al., 2017). We have constrained the age model of MPG ice using nine ^{14}C absolute dating from different materials (Table 3), the absence of ^{137}C and ^{210}Pb in surface ice samples and integrating in the chronology the characteristics of the ice stratigraphy, such as the presence of dark debris-rich layers.

The age-depth model obtained indicates the presence of ice since 2000 years ago and allows distinguishing three main periods for MPG (Fig. 3). Period I was an accumulation period from 0 to 700 CE. Period II represents an ablation-dominated phase from 700 to 1200 CE, which corresponds to the dark-rich layer interval where more dates are concentrated. Period III corresponds to a new accumulation period from 1200 to 1400 CE. This period agrees well with an increase in cold season (Oct–May) heavy rainfall events in the Southern Central Pyrenees between 1164 – 1414 CE (Corella et al., 2016) that most likely resulted on higher snow accumulation at high elevation areas, leading to a net accumulation in MPG. Finally, no ice formed during, at least, the last 600 years has been found today in MPG. This indicates that the LIA ice has been melted away, pointing to an intense ablation period since 1850 CE. The MPG age model is supported by, first, a quantitative comparison with present-day atmospheric particulate matter (Table 4) and, second, by the comparison with the paleoenvironmental sequence of

383 the Marboré Lake for the last 2000 years (Corella et al., 2021; Oliva-Urcia et al., 2018)
384 (Fig. 4).

385 Present-day aerosols in the studied region are well-recorded ^{at the nearby} ~~in~~ Ordesa site (Pey et al.,
386 2020). Following previous studies on present-day atmospheric particulate matter
387 composition from natural, urban or industrial areas (Querol et al., 2007), the values of
388 some elemental ratios (e.g., Cu/Mn, As/Se, Pb/Zn) help to determine the origin of the
389 particulate matter accumulated today. The Ordesa site can accordingly be mostly
390 defined as remote in terms of atmospheric deposition (“rural background”) while the
391 average composition of MPG ice samples could be defined as a site under the influence
392 of Cu mining and smelting activities, due to the high values of the Cu/Mn, As/Se and
393 Pb/Zn ratios. It is noteworthy that Cu, Ag, and Pb mining and smelting have been
394 historically documented in Bielsa valley during pre-industrial times (Callén, 1996).
395 Indeed, MPG is only 7 km east from some of the largest lead and silver ore deposits in
396 the Central Pyrenees (historical mines of Parzán). The impact of ancient environmental
397 pollution in high alpine environments is archived in the lacustrine sequence of the
398 neighbouring Marboré Lake, providing first evidences of long-range transport of trace
399 metals from historical metal mining and smelting activities during the Roman Period
400 (RP) (Corella et al., 2018, 2021). Similar ice core records from the Alps have also
401 demonstrated the suitability of glacier ice to record local and regional mining and
402 smelting activities during RP and pre-Roman times (More et al., 2017; Preunkert et al.,
403 2019). Even if the enrichment of trace elements in MPG ice record may correspond to
404 mining activities during ancient times, the different altitude of MPG glacier with
405 respect to records from Alpine glaciers where such activities were recorded (> 4000m
406 a.s.l.), together with the likely processes of redistribution of chemical impurities due to
407 percolation (Pohjola et al., 2002), prevents a firm interpretation of the origin of these
408 elements.

409 On the other hand, the comparison of Pb/Al ratios from the independently dated
410 records of Marboré Lake and MPG provides further support to the obtained glacier
411 chronology (Fig. 4). In particular, the lack of a Pb/Al peak characterizing the Industrial
412 Period in the upper sequence of the MPG confirms the absence of the last two
413 centuries in MPG ice record, in agreement with the ²¹⁰Pb and ¹³⁷Cs analyses  milarly,

the Hg concentration in the glacier is very stable throughout the ice sequence (Fig.4). Hg concentrations in other ice core records show an increase during the onset of Industrialization at 1800 CE with maximum values typically 3–10 times higher than preindustrial values (Cooke et al., 2020). In Marboré Lake, the Hg increase occurred over the last 500 years associated to the maximum activity in the Spanish Almadén mines during the Colonial Period (Corella et al., 2021). Again, these results, lacking an expected increase in Hg levels, support the age model from the MPG record where the last six centuries of ice deposition are missing.

5.2. Evolution of the Monte Perdido glacier over the last 2000 years

The analyzed ice from MPG provides valuable information about the evolution of the glacier during the last two millennia, which deserves consideration in the regional context. Based on published results, the oldest paleoclimatic information in the Marboré Cirque comes from the Marboré Lake, since no glacier deposits corresponding to the Late Pleistocene have been found in the cirque (García-Ruiz et al., 2014). There is sedimentological evidence that the Marboré Lake was already ice-free at least since the onset of the Bølling period (Greenland Interstadial-1, 14,600 yr BP), when clastic sediments were deposited in the lake basin (Leunda et al., 2017; Oliva-Urcia et al., 2018). This is coherent with the nearby La Larri *juxta-glacial* sequence which showed that the main Pineta glacier had already retreated further up in the headwater by 11 kyr BP (Salazar et al., 2013). In fact, glaciological studies performed in the Central Pyrenees confirm the sudden retreat of glaciers during the Bølling period, when they were reduced to small ice tongues or cirque glaciers (Palacios et al., 2017). The next piece of information comes from the outermost moraine that was dated at 6900 ± 800 ^{36}Cl yr BP (García-Ruiz et al., 2020), corresponding to the Neoglacial advance, a cold period identified in the sediments of Marbore Lake (Leunda et al., 2017). Other minor advances would have occurred in MPG prior to the LIA, as inferred from three polished surfaces dated at 3500 ± 400 , 2500 ± 300 and 1100 ± 100 ^{36}Cl yr BP (García-Ruiz et al., 2020).

With the new chronology of the MPG record, we can ascertain that MPG has persisted at least since the RP (ca. 2000 years ago). At that time, which is a well-known warm

444 period in the Iberian Peninsula as recorded in both continental (Martín-Puertas et al.,
445 2010; Morellón et al., 2009) and marine sequences (Cisneros et al., 2016; Margaritelli
446 et al., 2020), the glacier was still present, but probably smaller than during previous
447 Neoglacial times (Fig. 5B). This situation probably continued during the following cold
448 period, the Dark Ages (DA, Fig 5C) when the glacier advanced as indicated by the
449 polished surface dated at 1100 ± 100 ^{36}Cl yr BP (García-Ruiz et al., 2020). In the Alps,
450 reconstructions based on dating trees found within and at the edge of glacier forefields
451 have revealed a minimum glacier extent during the Iron Age and the RP (Holzhauser et
452 al., 2005), when glaciers were estimated to be smaller than during the 1920s (Ivy-Ochs
453 et al., 2009). Afterwards, in the late RP and the early Middle Ages numerous glaciers in
454 the Alps advanced during the DA, also known as the Göschenen II oscillation
455 (Holzhauser et al., 2005).

456 The MCA (900–1300 CE) is the most recent preindustrial warm era in Europe (Mann et
457 al., 2009). For instance, in the Alps, a general glacier retreat has been observed during
458 this period, mainly associated with a decline in precipitation (Holzhauser et al., 2005).
459 According to the age-depth model, the MPG experienced a spectacular retreat (Fig.
460 5D), including the complete melting of some minor glaciers in the Marboré Cirque
461 (García-Ruiz et al., 2020). Nevertheless, during the MCA part of MPG was preserved, as
462 we find ice from 0 to 700 CE. No doubt the ice loss was significant, as evidenced by the
463 accumulation of dark strata over a long time interval (600 – 1200 CE) (Fig.3). On this
464 basis, we propose that the MPG was dominated by ablation processes during the MCA,
465 leading to considerable ice loss and reduced from just six meters of ice remaining from
466 this period (blue horizontal line, Fig. 3). It is evident that at the end of the MCA the
467 MPG still preserved ice from the RP and the first half of the DA (Fig. 5D). It is difficult to
468 assure if Neoglacial basal ice is still present in MPG since no ice sample was dated with
469 Neoglacial age or even older. Still, Neoglacial ice can remain in the glacier base without
470 being exposed by the slope where sampling procedures were carried out.

471 Over such a diminished MCA glacier, ice started to accumulate again at a rapid rate
472 during the LIA (1300 – 1850 CE). In most cases, the LIA was the period when mountain
473 glaciers recorded their maximum Holocene extent (Solomina et al., 2016), with
474 remarkable advances in the alpine glaciers (Ivy-Ochs et al., 2009). From a large variety

of proxies, several warm and cold periods have been identified in the Iberian Peninsula during the LIA (Oliva et al., 2018). In the Marboré Cirque two generations of LIA moraines have been mapped (García-Ruiz et al., 2014), whose emplacement coincided with the coldest LIA phases, i.e. 1620 - 1715 CE, when the Pyrenean glaciers recorded their maximum extent of the last two millennia, and at some time between 1820 - 1840 CE, when a rapid advance of the ice mass moved over the large moraine leaving parallel ridges and furrows, so-called flutes, as signs of erosion (García-Ruiz et al., 2020; Serrano and Martín-Moreno, 2018). These two cold phases are very well identified in the Marboré Cirque and were confirmed by the study of the altitudinal fluctuations of the timberline in the neighboring Escuaín Valley (Camarero et al., 2015). In fact, according to the map of Schrader from 1874 CE and other historical sources, the MPG made direct contact with the large moraine in the second half of the 19th century (García-Ruiz et al., 2014). Despite the fact that the MPG would have covered an area of 5.56 km² at the end of the LIA (in 1894 (González Trueba et al., 2008), Fig. 5E), there is no record today of ice accumulated during the LIA, except for a few meters at the top of the sequence corresponding to about 1400 CE. This means that more than 600 years of ice accumulation have been lost associated to the warming after ca. 1850 CE. This situation is not so common in the Alps, where ice from the LIA, and even from the last two centuries, is still preserved in many studied cold glaciers (Eichler et al., 2000; Gabrielli et al., 2016; Gäggeler et al., 1983; Preunkert et al., 2019).

Today the MPG is divided in two small ice bodies that together cover just 0.38 km² (López-Moreno et al., 2016, Fig. 5F). Comparing the MPG extent at the end of the LIA (ca. 1850 CE), as given by the moraine location, and today's extent, more than 5 km² of MPG would have disappeared, thus indicating that the last 150 years have likely been the period with the largest glacier melting over the last 2000 years.

5. Conclusions

This study presents for the first time a continuous chronological model of a remaining small glacier in the Pyrenees, reconstructed from a set of ¹⁴C dates on different organic remains, and supported by measurements of current atmospheric deposition and comparison with a nearby lake sequence (Marboré Lake). The ice sequence from MPG

covers the last 2000 years, allowing the identification of cold time periods of growing glaciers and warm time periods of ice loss. We demonstrate that the glacier was active during the RP, a well-known warm period in the Iberian Peninsula. During the MCA, the MPG experienced a spectacular retreat marked by the presence of dark debris layers indicative of successive years when ablation processes predominated. The LIA was a period of glacier growth but is not recorded today in the ice from MPG, since more than 600 years of ice accumulation have been lost associated to the warming after the end of the LIA, ca. 1850 CE. This evidence from the age-depth model is supported by the lack of anthropogenic indicators usually associated to the Industrial Era abundant today in current atmospheric deposition in a nearby site. Additionally, both Hg concentration and Pb/Al ratio appear much higher in the Marboré Lake sediments, whereas the MPG record does not reflect their anthropogenic increase.

Comparing the present-day glacier situation with that of previous warm intervals, such as the RP or the MCA, we conclude that the MPG is nowadays greatly reduced in area and volume. Additionally, the recent rate of ice-mass loss is definitely more rapid than that of the four centuries spanned by the MCA, thus suggesting that present day warming in the Pyrenees is faster and more intense than in any previous warm phase of the last 2000 years. Under the current climatic conditions, it is reasonable to expect the disappearance of this glacier, as well as other glaciers in the Pyrenees and in Southern Europe, over the next few decades.

6. Data availability

The input data file for CLAM as well as the output results are stored in the open repository Zenodo (<https://zenodo.org/record/3886911>). The rest of data are given in the paper Tables.

7. Author contributions

The paper was conceived by A.M., M.B., C.S. and J.I.L-M. together with F.N., J.O-G., J.L., P.G-S., C.C., J.L-M., B.O-U, S.H.F and J.G-R. who contributed to design and develop this research project (PaleoICE). F.N., C.P., M.L., E.A. participated during field work to recover the samples; A.M., M.B. and M.L. prepared the samples for ¹⁴C dating; J.G.O.

carried out the ^{210}Pb and ^{137}Cs analyses; J.P., X.Q. and A.A. provided the geochemical data from Ordesa site and MPG; J.P.C., M.J.S. and R.M. provided the Hg data from Marboré Lake and MPG; and G.G.-R. built the age depth-model. All authors contributed to discuss and interpret the data and to the writing of the original and revised version of this paper.

8. Competing interest

The authors declare that they have no conflict of interest.

9. Acknowledgements

The Spanish Agencia Estatal de Investigación (AEI – Spain) and the European Funds for Regional Development (FEDER – European Union) are gratefully acknowledged for financial support through PaleolCE EXPLORA project (CGL2015-72167-EXP), CGL2015-68993-R, CGL2015-69160-R and CTM2017-84441-R projects (AEI/FEDER, UE) and through the iMechPro RETOS project (RTI2018-100696-B-I00). S.H.F. and J.G.-O. acknowledge support by the Spanish Government through María de Maeztu excellence accreditation 2018-2022 ref MDM-2017-0714 and ref CEX-2019-000940-M, respectively. M.B. is supported by postdoctoral fellowship Juan de la Cierva-Formación program provided by the Spanish Ministry of Science, Innovation and Universities (ref.: FJCI-2017-34235063753). The authors are grateful to Eduardo Bartolomé and José Estebán Lozano for their help manufacturing parts of the coring devices and to the support provided by the Dirección General de Conservación del Medio Natural (Government of Aragón) and by the staff of the Ordesa and Monte Perdido National Park during our field campaigns. This study contributes to the work carried out by the GA research group Procesos Geoambientales y Cambio Global (ref E02-20R) and MERS research group 2017 SGR 1588.

10. References

- Blaauw, M.: Methods and code for ‘classical’ age-modelling of radiocarbon sequences, *Quaternary Geochronology*, 5(5), 512–518, doi:10.1016/j.quageo.2010.01.002, 2010.
- Blaauw, M., Christen, J. A., Vázquez, J. E. and Goring, S.: clam: Classical Age-Depth Modelling of Cores from Deposits. CRAN 2019, [online] Available from: <https://CRAN.R-project.org/package=clam>, 2019.

564 Bohleber, P.: Alpine Ice Cores as Climate and Environmental Archives, Oxford Research
565 Encyclopedia of Climate Science, doi:10.1093/acrefore/9780190228620.013.743, 2019.

566 Büntgen, U., Krusic, P. J., Verstege, A., Sangüesa-Barreda, G., Wagner, S., Camarero, J. J.,
567 Ljungqvist, F. C., Zorita, E., Oppenheimer, C., Konter, O., Tegel, W., Gärtner, H., Cherubini, P.,
568 Reinig, F. and Esper, J.: New Tree-Ring Evidence from the Pyrenees Reveals Western
569 Mediterranean Climate Variability since Medieval Times, *J. Climate*, 30(14), 5295–5318,
570 doi:10.1175/JCLI-D-16-0526.1, 2017.

571 Callén, J. J. N.: El proceso sidero-metarlúrgico altoaragonés: los valles de Bielsa y Gistain en la
572 Edad Moderna (1565-1800), *Llull: Revista de la Sociedad Española de Historia de las Ciencias y*
573 *de las Técnicas*, 19(37), 471–508, 1996.

574 Camarero, J. J., García-Ruiz, J. M., Sangüesa-Barreda, G., Galván, J. D., Alla, A. Q., Sanjuán, Y.,
575 Beguería, S. and Gutiérrez, E.: Recent and Intense Dynamics in a Formerly Static Pyrenean
576 Treeline, *Arctic, Antarctic, and Alpine Research*, 47(4), 773–783, doi:10.1657/AAAR0015-001,
577 2015.

578 Cisneros, M., Cacho, I., Frigola, J., Canals, M., Masqué, P., Martrat, B., Casado, M., Grimalt, J.
579 O., Pena, L. D., Margaritelli, G. and Lirer, F.: Sea surface temperature variability in the central-
580 western Mediterranean Sea during the last 2700 years: a multi-proxy and multi-record
581 approach, *Clim. Past*, 12(4), 849–869, doi:10.5194/cp-12-849-2016, 2016.

582 Cooke, C. A., Martínez-Cortizas, A., Bindler, R. and Sexauer Gustin, M.: Environmental archives
583 of atmospheric Hg deposition – A review, *Science of The Total Environment*, 709, 134800,
584 doi:10.1016/j.scitotenv.2019.134800, 2020.

585 Corella, J. P., Valero-Garcés, B. L., Vicente- Serrano, S. M., Brauer, A. and Benito, G.: Three
586 millennia of heavy rainfalls in Western Mediterranean: frequency, seasonality and atmospheric
587 drivers, *Scientific Reports*, 6(1), doi:10.1038/srep38206, 2016.

588 Corella, J. P., Saiz-Lopez, A., Sierra, M. J., Mata, M. P., Millán, R., Morellón, M., Cuevas, C. A.,
589 Moreno, A. and Valero-Garcés, B. L.: Trace metal enrichment during the Industrial Period
590 recorded across an altitudinal transect in the Southern Central Pyrenees, *Science of The Total*
591 *Environment*, 645, 761–772, doi:10.1016/j.scitotenv.2018.07.160, 2018.

592 Corella, J. P., Sierra, M. J., Garralón, A., Millán, R., Rodríguez-Alonso, J., Mata, M. P., de Vera, A.
593 V., Moreno, A., González-Sampériz, P., Duval, B., Amouroux, D., Vivez, P., Cuevas, C. A., Adame,
594 J. A., Wilhelm, B., Saiz-Lopez, A. and Valero-Garcés, B. L.: Recent and historical pollution legacy
595 in high altitude Lake Marboré (Central Pyrenees): A record of mining and smelting since pre-
596 Roman times in the Iberian Peninsula, *Science of The Total Environment*, 751, 141557,
597 doi:10.1016/j.scitotenv.2020.141557, 2021.

598 Davis, P. T., Menounos, B. and Osborn, G.: Holocene and latest Pleistocene alpine glacier
599 fluctuations: a global perspective, *Quaternary Science Reviews*, 28(21–22), 2021–2033,
600 doi:10.1016/j.quascirev.2009.05.020, 2009.

601 Eichler, A., Schwikowski, M., Gäggeler, H. W., Furrer, V., Synal, H.-A., Beer, J., Saurer, M. and
602 Funk, M.: Glaciochemical dating of an ice core from upper Grenzgletscher (4200 m a.s.l.),
603 *Journal of Glaciology*, 46(154), 507–515, doi:10.3189/172756500781833098, 2000.

604 Ewing, M. E., Reese, C. A. and Nolan, M. A.: The potential effects of percolating snowmelt on
605 palynological records from firn and glacier ice, *Journal of Glaciology*, 60(222), 661–669,
606 doi:10.3189/2014JoG13J158, 2014.

607 Festi, D., Carturan, L., Kofler, W., dalla Fontana, G., de Blasi, F., Cazorzi, F., Bucher, E., Mair, V.,
608 Gabrielli, P. and Oeggli, K.: Linking pollen deposition and snow accumulation on the Alto
609 dell’Ortles glacier (South Tyrol, Italy) for sub-seasonal dating of a firn temperate core, *The*
610 *Cryosphere*, 11(2), 937–948, doi:10.5194/tc-11-937-2017, 2017.

611 Fletcher, W. J., Zielhofer, C., Mischke, S., Bryant, C., Xu, X. and Fink, D.: AMS radiocarbon
612 dating of pollen concentrates in a karstic lake system, *Quaternary Geochronology*, 39, 112–
613 123, doi:10.1016/j.quageo.2017.02.006, 2017.

614 Gabrielli, P., Barbante, C., Bertagna, G., Bertó, M., Binder, D., Carton, A., Carturan, L., Cazorzi,
615 F., Cozzi, G., Dalla Fontana, G., Davis, M., De Blasi, F., Dinale, R., Dragà, G., Dreossi, G., Festi, D.,
616 Frezzotti, M., Gabrieli, J., Galos, S. P., Ginot, P., Heidenwolf, P., Jenk, T. M., Kehrwald, N.,
617 Kenny, D., Magand, O., Mair, V., Mikhalenko, V., Lin, P. N., Oeggli, K., Piffer, G., Rinaldi, M.,
618 Schotterer, U., Schwikowski, M., Seppi, R., Spolaor, A., Stenni, B., Tonidandel, D., Uglietti, C.,
619 Zagorodnov, V., Zanoner, T. and Zennaro, P.: Age of the Mt. Ortles ice cores, the Tyrolean
620 Iceman and glaciation of the highest summit of South Tyrol since the Northern Hemisphere
621 Climatic Optimum, *The Cryosphere*, 10(6), 2779–2797, doi:10.5194/tc-10-2779-2016, 2016.

622 Gäggeler, H., Gunten, H. R. von, Rössler, E., Oeschger, H. and Schotterer, U.: 210Pb-Dating of
623 Cold Alpine Firn/Ice Cores From Colle Gnifetti, Switzerland, *Journal of Glaciology*, 29(101),
624 165–177, doi:10.1017/S00222143000005220, 1983.

625 García-Ruiz, J. M., Palacios, D., Andrés, N. de, Valero-Garcés, B. L., López-Moreno, J. I. and
626 Sanjuán, Y.: Holocene and ‘Little Ice Age’ glacial activity in the Marboré Cirque, Monte Perdido
627 Massif, Central Spanish Pyrenees, *The Holocene*, 0959683614544053,
628 doi:10.1177/0959683614544053, 2014.

629 García-Ruiz, J. M., Palacios, D., Andrés, N. and López-Moreno, J. I.: Neoglaciation in the Spanish
630 Pyrenees: a multiproxy challenge, *Med. Geosc. Rev.*, 2(1), 21–36, doi:10.1007/s42990-020-
631 00022-9, 2020.

632 Garzonio, R., Di Mauro, B., Strigaro, D., Rossini, M., Colombo, R., De Amicis, M. and Maggi, V.:
633 Mapping the suitability for ice-core drilling of glaciers in the European Alps and the Asian High
634 Mountains, *J. Glaciol.*, 64(243), 12–26, doi:10.1017/jog.2017.75, 2018.

635 González Trueba, J. J., Moreno, R. M., Martínez de Pisón, E. and Serrano, E.: ‘Little Ice Age’
636 glaciation and current glaciers in the Iberian Peninsula, *The Holocene*, 18(4), 551–568,
637 doi:10.1177/0959683608089209, 2008.

638 Haeberli, W., Frauenfelder, R., Kääb, A. and Wagner, S.: Characteristics and potential climatic
639 significance of “miniature ice caps” (crest- and cornice-type low-altitude ice archives), *Journal*
640 *of Glaciology*, 50(168), 129–136, doi:10.3189/172756504781830330, 2004.

641 Herren, P.-A., Eichler, A., Machguth, H., Papina, T., Tobler, L., Zapf, A. and Schwikowski, M.: The
642 onset of Neoglaciation 6000 years ago in western Mongolia revealed by an ice core from the
643 Tsambagarav mountain range, *Quaternary Science Reviews*, 69, 59–68,
644 doi:10.1016/j.quascirev.2013.02.025, 2013.

645 Holzhauser, H., Magny, M. and Zumbühl, H. J.: Glacier and lake-level variations in west-central
646 Europe over the last 3500 years, *The Holocene*, 15(6), 789–801, 2005.

647 Hughes, P. D.: Little Ice Age glaciers and climate in the Mediterranean mountains: a new
648 analysis, *CIG*, 44(1), 15, doi:10.18172/cig.3362, 2018.

649 Ivy-Ochs, S., Kerschner, H., Maisch, M., Christl, M., Kubik, P. W. and Schlüchter, C.: Latest
650 Pleistocene and Holocene glacier variations in the European Alps, *Quaternary Science Reviews*,
651 28(21–22), 2137–2149, doi:10.1016/j.quascirev.2009.03.009, 2009.

652 Jenk, T. M., Szidat, S., Bolius, D., Sigl, M., Gäggeler, H. W., Wacker, L., Ruff, M., Barbante, C.,
653 Boutron, C. F. and Schwikowski, M.: A novel radiocarbon dating technique applied to an ice
654 core from the Alps indicating late Pleistocene ages, *Journal of Geophysical Research:*
655 *Atmospheres*, 114(D14), doi:10.1029/2009JD011860, 2009.

656 Kilian, M. R., van der Plicht, J., van Geel, B. and Goslar, T.: Problematic ¹⁴C-AMS dates of pollen
657 concentrates from Lake Gosciaz (Poland), *Quaternary International*, 88(1), 21–26,
658 doi:10.1016/S1040-6182(01)00070-2, 2002.

659 Leunda, M., González-Sampériz, P., Gil-Romera, G., Aranbarri, J., Moreno, A., Oliva-Urcia, B.,
660 Sevilla-Callejo, M. and Valero-Garcés, B.: The Late-Glacial and Holocene Marboré Lake
661 sequence (2612m a.s.l., Central Pyrenees, Spain): Testing high altitude sites sensitivity to
662 millennial scale vegetation and climate variability, *Global and Planetary Change*, 157, 214–231,
663 doi:10.1016/j.gloplacha.2017.08.008, 2017.

664 López-Moreno, J. I., Revuelto, J., Rico, I., Chueca-Cía, J., Julián, A., Serreta, A., Serrano, E.,
665 Vicente-Serrano, S. M., Azorin-Molina, C., Alonso-González, E. and García-Ruiz, J. M.: Thinning
666 of the Monte Perdido Glacier in the Spanish Pyrenees since 1981, *The Cryosphere*, 10(2), 681–
667 694, doi:10.5194/tc-10-681-2016, 2016.

668 López-Moreno, J. I., Alonso-González, E., Monserrat, O., Del Río, L. M., Otero, J., Lapazaran, J.,
669 Luzi, G., Dematteis, N., Serreta, A., Rico, I., Serrano-Cañadas, E., Bartolomé, M., Moreno, A.,
670 Buisan, S. and Revuelto, J.: Ground-based remote-sensing techniques for diagnosis of the
671 current state and recent evolution of the Monte Perdido Glacier, Spanish Pyrenees, *J. Glaciol.*,
672 65(249), 85–100, doi:10.1017/jog.2018.96, 2019.

673 Mann, M. E., Zhang, Z., Rutherford, S., Bradley, R. S., Hughes, M. K., Shindell, D., Ammann, C.,
674 Faluvegi, G. and Ni, F.: Global Signatures and Dynamical Origins of the Little Ice Age and
675 Medieval Climate Anomaly, *Science*, 326(5957), 1256–1260, 2009.

676 Margaritelli, G., Cacho, I., Català, A., Barra, M., Bellucci, L. G., Lubritto, C., Rettori, R. and Lirer,
677 F.: Persistent warm Mediterranean surface waters during the Roman period, *Scientific Reports*,
678 10(1), 10431, doi:10.1038/s41598-020-67281-2, 2020.

679 Martín-Puertas, C., Jiménez-Espejo, F., Martínez-Ruiz, F., Nieto-Moreno, V., Rodrigo, M., Mata,
680 M. P. and Valero-Garcés, B. L.: Late Holocene climate variability in the southwestern
681 Mediterranean region: an integrated marine and terrestrial geochemical approach, *Clim. Past*,
682 6(6), 807–816, doi:10.5194/cp-6-807-2010, 2010.

683 Marzeion, B., Cogley, J. G., Richter, K. and Parkes, D.: Attribution of global glacier mass loss to
684 anthropogenic and natural causes, *Science*, 345(6199), 919–921,
685 doi:10.1126/science.1254702, 2014.

686 Moore, P. D., Webb, J. A. and Collinson, M. E.: Pollen Analysis, Second., Blackwell Scientific
687 Publications., 1991.

688 More, A. F., Spaulding, N. E., Bohleber, P., Handley, M. J., Hoffmann, H., Korotkikh, E. V.,
689 Kurbatov, A. V., Loveluck, C. P., Sneed, S. B., McCormick, M. and Mayewski, P. A.: Next-
690 generation ice core technology reveals true minimum natural levels of lead (Pb) in the
691 atmosphere: Insights from the Black Death, *GeoHealth*, 1(4), 211–219,
692 doi:10.1002/2017GH000064, 2017.

693 Morellón, M., Valero-Garcés, B., Vegas-Vilarrúbia, T., González-Sampériz, P., Romero, Ó.,
694 Delgado-Huertas, A., Mata, P., Moreno, A., Rico, M. and Corella, J. P.: Lateglacial and Holocene
695 palaeohydrology in the western Mediterranean region: The Lake Estanya record (NE Spain),
696 *Quaternary Science Reviews*, 28(25–26), 2582–2599, 2009.

697 Oerlemans, J.: *Glaciers and Climate Change*, CRC Press., 2001.

698 Oliva, M., Ruiz-Fernández, J., Barriendos, M., Benito, G., Cuadrat, J. M., Domínguez-Castro, F.,
699 García-Ruiz, J. M., Giral, S., Gómez-Ortiz, A., Hernández, A., López-Costas, O., López-Moreno,
700 J. I., López-Sáez, J. A., Martínez-Cortizas, A., Moreno, A., Prohom, M., Saz, M. A., Serrano, E.,
701 Tejedor, E., Trigo, R., Valero-Garcés, B. and Vicente-Serrano, S. M.: The Little Ice Age in Iberian
702 mountains, *Earth-Science Reviews*, 177, 175–208, doi:10.1016/j.earscirev.2017.11.010, 2018.

703 Oliva-Urcia, B., Moreno, A., Leunda, M., Valero-Garcés, B., González-Sampériz, P., Gil-Romera,
704 G., Mata, M. P. and Group, H.: Last deglaciation and Holocene environmental change at high
705 altitude in the Pyrenees: the geochemical and paleomagnetic record from Marboré Lake (N
706 Spain), *J Paleolimnol*, 59(3), 349–371, doi:10.1007/s10933-017-0013-9, 2018.

707 Palacios, D., García-Ruiz, J. M., Andrés, N., Schimmelpfennig, I., Campos, N., Léanni, L.,
708 Aumaître, G., Bourlès, D. L. and Keddadouche, K.: Deglaciation in the central Pyrenees during
709 the Pleistocene–Holocene transition: Timing and geomorphological significance, *Quaternary
710 Science Reviews*, 162, 111–127, doi:10.1016/j.quascirev.2017.03.007, 2017.

711 Pey, J., Pérez, N., Cortés, J., Alastuey, A. and Querol, X.: Chemical fingerprint and impact of
712 shipping emissions over a western Mediterranean metropolis: Primary and aged contributions,
713 *Science of The Total Environment*, 463–464, 497–507, doi:10.1016/j.scitotenv.2013.06.061,
714 2013.

715 Pey, J., Larrasoana, J. C., Pérez, N., Cerro, J. C., Castillo, S., Tobar, M. L., de Vergara, A.,
716 Vázquez, I., Reyes, J., Mata, M. P., Mochales, T., Orellana, J. M. and Causapé, J.:
717 Phenomenology and geographical gradients of atmospheric deposition in southwestern
718 Europe: Results from a multi-site monitoring network, *Science of The Total Environment*, 744,
719 140745, doi:10.1016/j.scitotenv.2020.140745, 2020.

720 Pohjola, V. A., Moore, J. C., Isaksson, E., Jauhiainen, T., Wal, R. S. W. van de, Martma, T.,
721 Meijer, H. a. J. and Vaikmäe, R.: Effect of periodic melting on geochemical and isotopic signals
722 in an ice core from Lomonosovfonna, Svalbard, *Journal of Geophysical Research: Atmospheres*,
723 107(D4), ACL 1-1-ACL 1-14, doi:10.1029/2000JD000149, 2002.

724 Preunkert, S., McConnell, J. R., Hoffmann, H., Legrand, M., Wilson, A. I., Eckhardt, S., Stohl, A.,
725 Chellman, N. J., Arienzo, M. M. and Friedrich, R.: Lead and Antimony in Basal Ice From Col du
726 Dome (French Alps) Dated With Radiocarbon: A Record of Pollution During Antiquity,
727 *Geophysical Research Letters*, 46(9), 4953–4961, doi:10.1029/2019GL082641, 2019.

728 Querol, X., Viana, M., Alastuey, A., Amato, F., Moreno, T., Castillo, S., Pey, J., de la Rosa, J.,
 729 Sánchez de la Campa, A., Artíñano, B., Salvador, P., García Dos Santos, S., Fernández-Patier, R.,
 730 Moreno-Grau, S., Negral, L., Minguillón, M. C., Monfort, E., Gil, J. I., Inza, A., Ortega, L. A.,
 731 Santamaría, J. M. and Zabalza, J.: Source origin of trace elements in PM from regional
 732 background, urban and industrial sites of Spain, *Atmospheric Environment*, 41(34), 7219–7231,
 733 doi:10.1016/j.atmosenv.2007.05.022, 2007.

734 Reimer, P. J., Bard, E., Bayliss, A., Beck, J. W., Blackwell, P. G., Ramsey, C. B., Buck, C. E., Cheng,
 735 H., Edwards, R. L., Friedrich, M. and others: IntCal13 and Marine13 radiocarbon age calibration
 736 curves 0–50,000 years cal BP, *Radiocarbon*, 55(4), 1869–1887, 2013.

737 Rico, I., Izagirre, E., Serrano, E. and López-Moreno, J. I.: Superficie glaciar actual en los Pirineos:
 738 Una actualización para 2016, *Pirineos*, 172(0), 029, doi:10.3989/Pirineos.2017.172004, 2017.

739 Salazar, A., Mata, M. P., Rico, M., Valero-Garcés, Oliva-Urcia, B. and Rubio, F. M.: El paleolago
 740 de La Larri (Valle de Pineta, Pirineos), *Cuadernos de Investigación Geográfica*, 39(1), 97–116,
 741 2013.

742 Sanchez-Cabeza, J. A., Masqué, P. and Ani-Ragolta, I.: ^{210}Pb and ^{210}Po analysis in sediments
 743 and soils by microwave acid digestion, *J Radioanal Nucl Chem*, 227(1), 19–22,
 744 doi:10.1007/BF02386425, 1998.

745 Serrano, E. and Martín-Moreno, R.: Surge glaciers during the Little Ice Age in the Pyrenees,
 746 *Cuadernos de Investigación Geográfica*, 44(1), 213–244, doi:10.18172/cig.3399, 2018.

747 Solomina, O. N., Bradley, R. S., Hodgson, D. A., Ivy-Ochs, S., Jomelli, V., Mackintosh, A. N.,
 748 Nesje, A., Owen, L. A., Wanner, H., Wiles, G. C. and Young, N. E.: Holocene glacier fluctuations,
 749 *Quaternary Science Reviews*, 111, 9–34, doi:10.1016/j.quascirev.2014.11.018, 2015.

750 Solomina, O. N., Bradley, R. S., Jomelli, V., Geirsdottir, A., Kaufman, D. S., Koch, J., McKay, N. P.,
 751 Masiokas, M., Miller, G., Nesje, A., Nicolussi, K., Owen, L. A., Putnam, A. E., Wanner, H., Wiles,
 752 G. and Yang, B.: Glacier fluctuations during the past 2000 years, *Quaternary Science Reviews*,
 753 149, 61–90, doi:10.1016/j.quascirev.2016.04.008, 2016.

754 Taylor, S. R. and McLennan, S. M.: The geochemical evolution of the continental crust, *Reviews*
 755 *of Geophysics*, 33, 241–265, 1995.

756 Uglietti, C., Zapf, A., Jenk, T. M., Sigl, M., Szidat, S., Salazar, G. and Schwikowski, M.:
 757 Radiocarbon dating of glacier ice: overview, optimisation, validation and potential, *The*
 758 *Cryosphere*, 10(6), 3091–3105, doi:10.5194/tc-10-3091-2016, 2016.

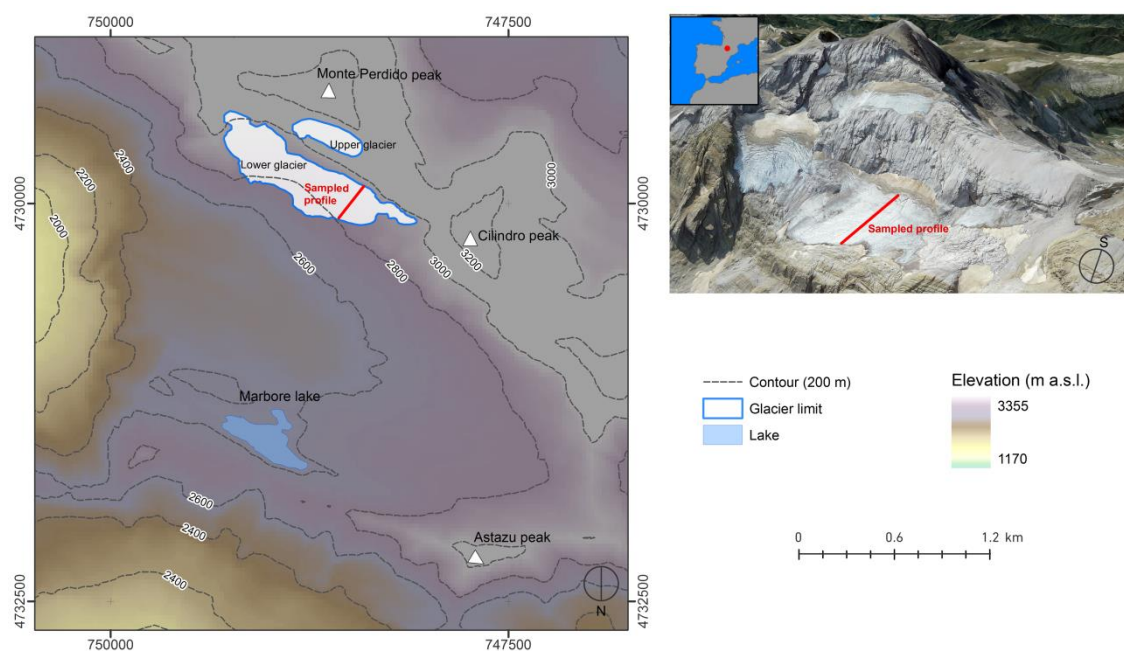
759 Wanner, H., Solomina, O., Grosjean, M., Ritz, S. P. and Jetel, M.: Structure and origin of
 760 Holocene cold events, *Quaternary Science Reviews*, 30(21–22), 3109–3123,
 761 doi:10.1016/j.quascirev.2011.07.010, 2011.

762 Zemp, M., Frey, H., Gärtner-Roer, I., Nussbaumer, S. U., Hoelzle, M., Paul, F., Haeberli, W.,
 763 Denzinger, F., Ahlstrøm, A. P., Anderson, B., Bajracharya, S., Baroni, C., Braun, L. N., Cáceres, B.
 764 E., Casassa, G., Cobos, G., Dávila, L. R., Granados, H. D., Demuth, M. N., Espizua, L., Fischer, A.,
 765 Fujita, K., Gadek, B., Ghazanfar, A., Hagen, J. O., Holmlund, P., Karimi, N., Li, Z., Pelto, M., Pitte,
 766 P., Popovnin, V. V., Portocarrero, C. A., Prinz, R., Sangewar, C. V., Severskiy, I., Sigurðsson, O.,
 767 Soruco, A., Usubaliev, R. and Vincent, C.: Historically unprecedented global glacier decline in
 768 the early 21st century, *Journal of Glaciology*, 61(228), 745–762, doi:10.3189/2015JoG15J017,
 769 2015.

770 Zemp, M., Huss, M., Thibert, E., Eckert, N., McNabb, R., Huber, J., Barandun, M., Machguth, H.,
771 Nussbaumer, S. U., Gärtner-Roer, I., Thomson, L., Paul, F., Maussion, F., Kutuzov, S. and Cogley,
772 J. G.: Global glacier mass changes and their contributions to sea-level rise from 1961 to 2016,
773 Nature, 568(7752), 382–386, doi:10.1038/s41586-019-1071-0, 2019.

774

775



776

777

778 **Figure 1.** (left) Location of Monte Perdido Glacier (MPG) within a digital elevation map
 779 of Marboré Cirque; (right) Picture (©Google Earth) of MPG where the location of the
 780 sampled profile is indicated (see Fig. 2).

781

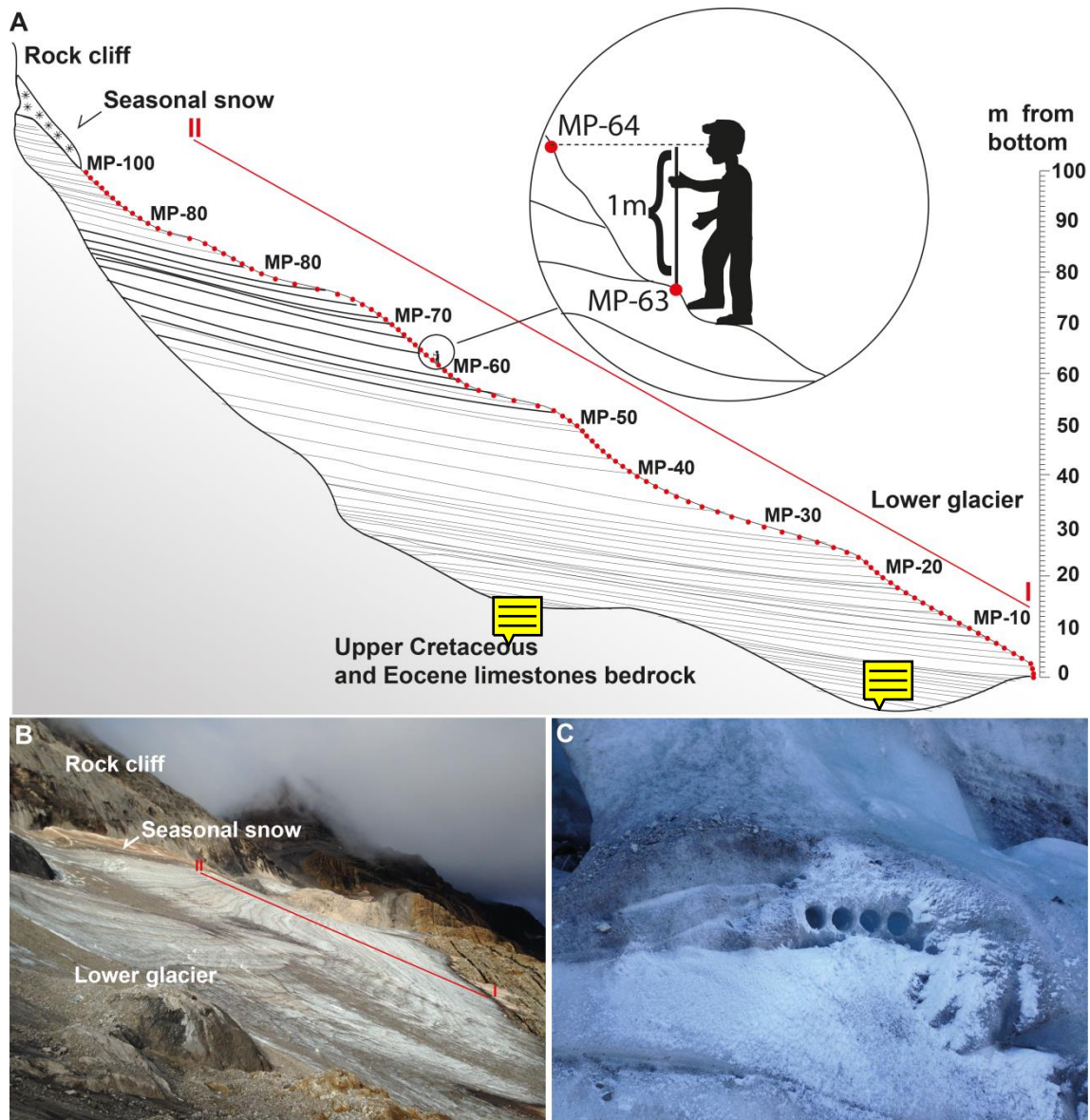
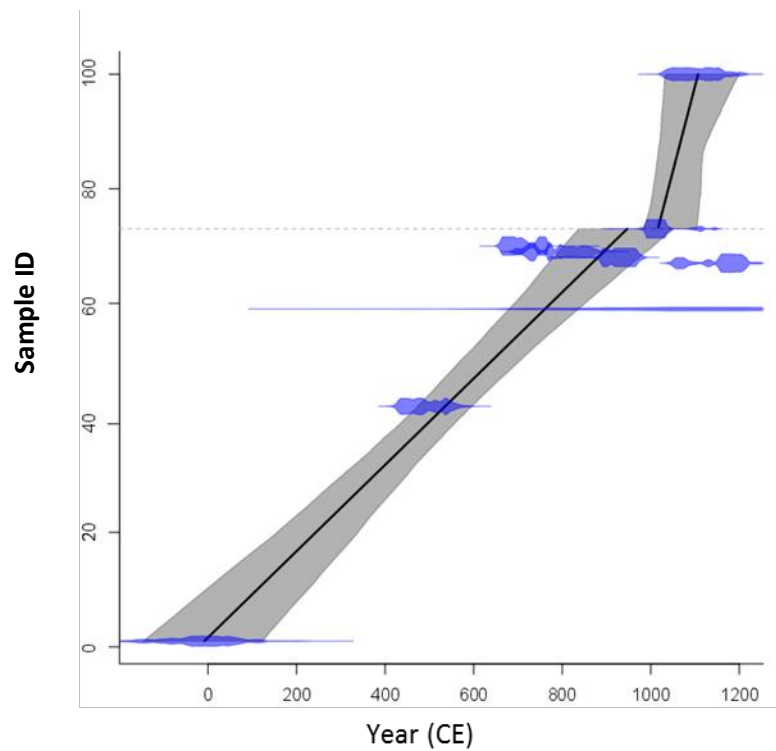


Figure 2. (A) Simplified scheme with the position of the 100 samples collected along the slope (red line I-II marks the profile indicated in B; identification of the samples is MP-0 to MP-100). According to the ice bedding (tilt is approximate) the oldest material should be found at the bottom of the lower glacier. Note the inset with a detailed view of the sampling procedure measuring a height difference of 1 m to obtain every sample. (B) Image of the Monte Perdido glacier surface where the sampling was carried out (red line I- II represents the sampled profile shown in Figure 1). Note the presence of dark debris-rich layers alternating with cleaner ice. (C). Detailed view indicating that every sample consisted in 3-4 small horizontally-drilled cylinders (see text for more details).

794



795

796 **Figure 3.** Age model for the Monte Perdido ice sequence based on linear interpolation
 797 of ^{14}C data (Table 3), obtained using the Clam software (Blaauw, 2010; Blaauw et al.,
 798 2019). Y axis indicates the number of samples from MP-0 to MP-100 (see Fig. 2). The
 799 dates appear as the calendar-age probability distributions in blue, while the black line
 800 is the resulting depth-age model and the gray envelope shows the 95 % confidence
 801 interval. Note the hiatus located at 73 m indicated by a dashed line. The error of
 802 sample MP59m is so high that appears as a horizontal line.

803

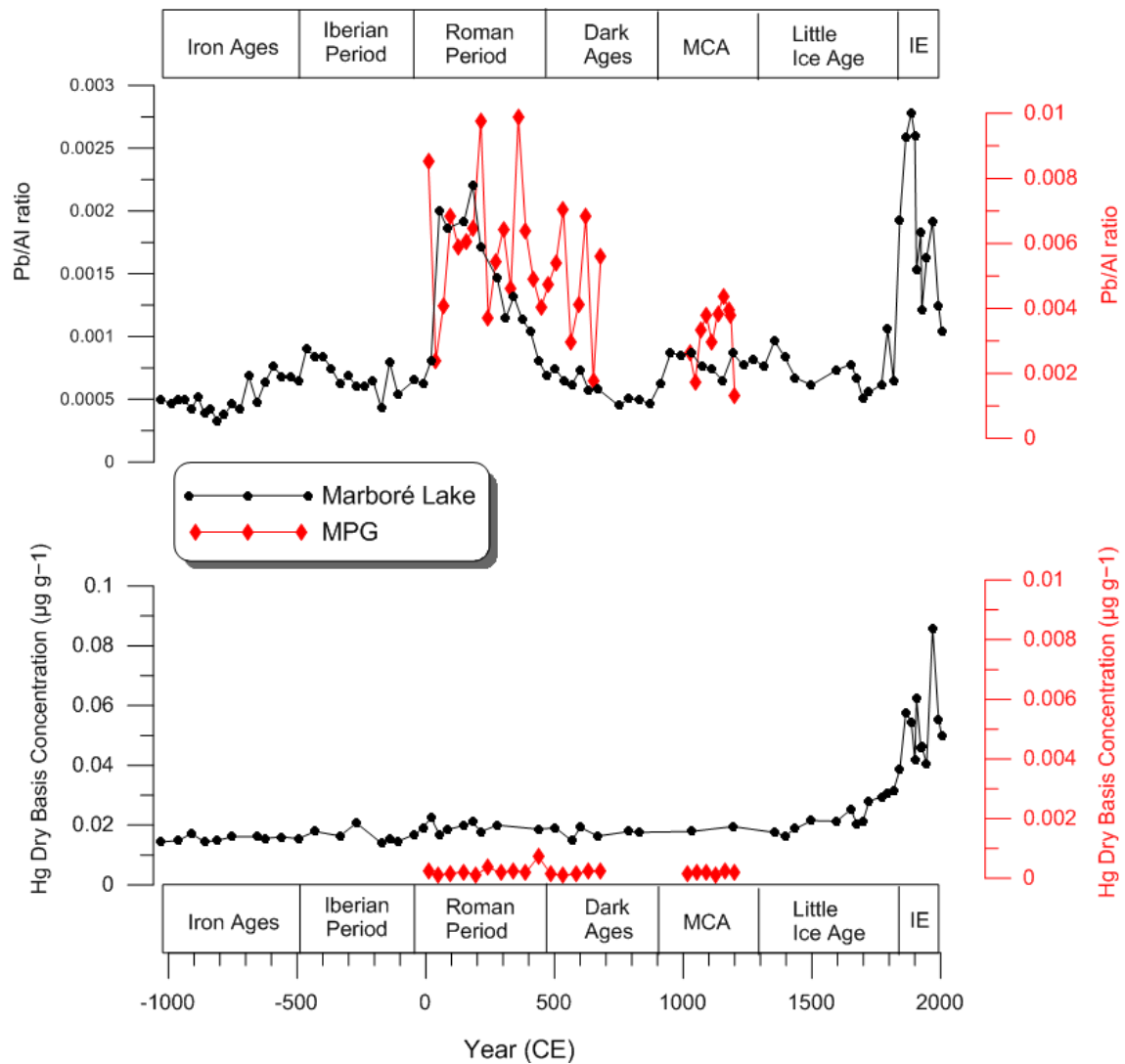


Figure 4. Comparison of Pb/Al ratio and Hg concentration of dry weight sediment in MPG samples with data obtained from Marboré Lake sediments (Corella et al., 2021). Note the differences in the vertical axis.

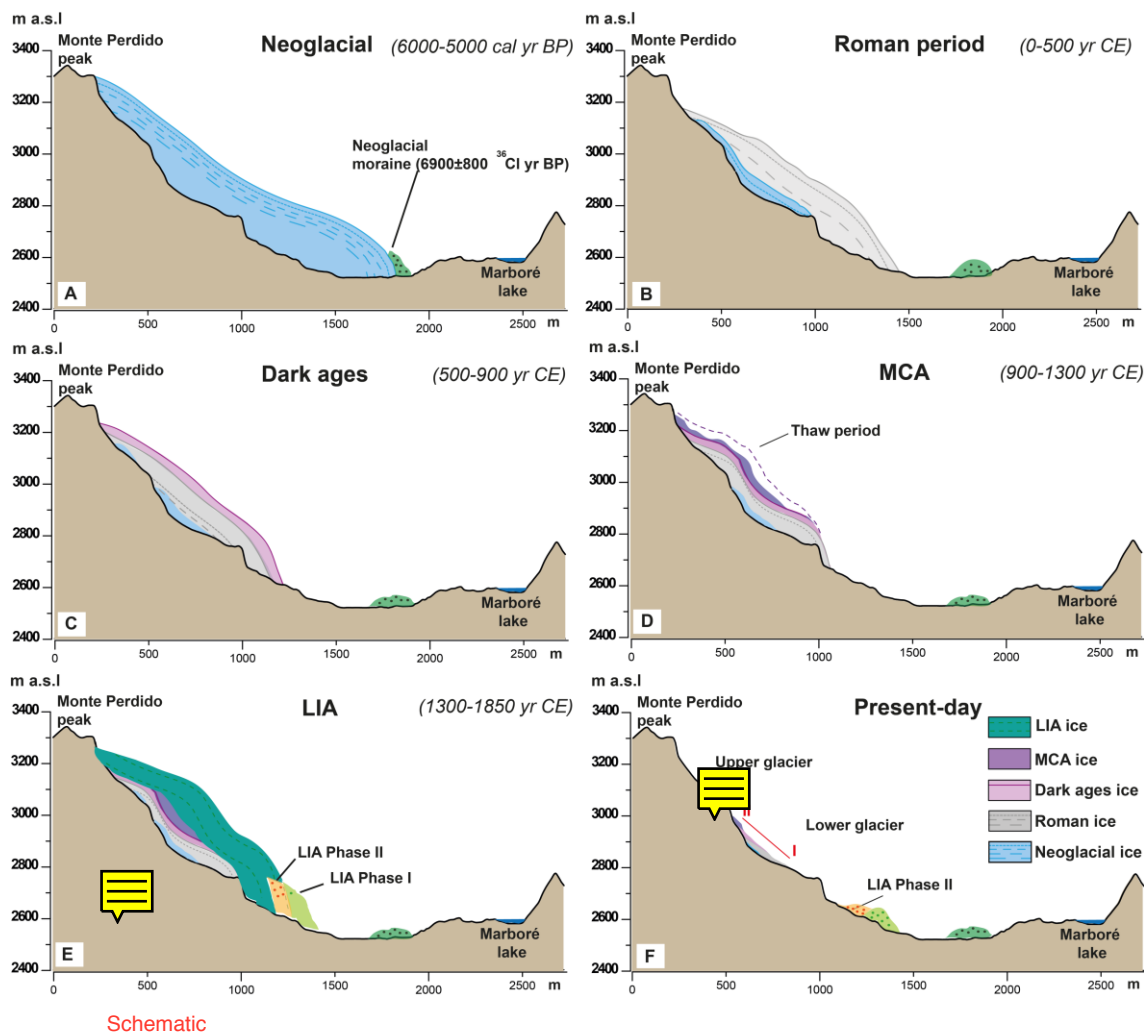


Figure 5. Geomorphic transects (south to north) taken from the Marboré Cirque, showing the tentative reconstruction of MPG during the six main stages discussed in the text. A) Neoglacial Period (ca. 5000 – 6000 cal yr BP) where the Neoglacial moraine is indicated (García-Ruiz et al., 2014); (B) Roman Period (0-500 CE) when the glacier is shown considerably retreated; (C) Dark Ages (500-900 CE); (D) Medieval Climate Anomaly (900-1300 CE), a period when the glacier retreated and ablation caused a concentration of debris and organic remains form dark layers in the glacier ice (discontinuous line aims to highlight the importance of melting processes); (E) Little Ice Age (1300-1850 CE), with the MPG reaching the LIA moraines position and (F) present-day situation characterized by the MPG divided into two ice bodies, no ice remaining from the LIA, and very steep slopes (sampling transect indicated by a red line).

822 **Table 1.** Concentrations of ^{137}Cs in the soluble water fraction of ice from Monte
823 Perdido samples.

Sample	Mass of ice analyzed (g)	MDA (Bq·L ⁻¹)
MP-61	240	0.15
MP-82	178	0.16
MP-97	232	0.14
MP-98	376	0.09
MP-100	238	0.17

824

825 **Table 2.** Determination of ^{210}Pb activity in the soluble water fraction of 100 g of ice
826 from Monte Perdido samples.

Sample	^{210}Pb activity (Bq·L ⁻¹)	MDA (Bq·L ⁻¹)
MP-73	17.4 ± 2.6	1.14
MP-76	6.2 ± 1.3	0.70
MP-82	<MDA	0.61
MP-85	<MDA	0.84
MP-88	<MDA	1.23
MP-91	<MDA	1.05
MP-94	<MDA	0.71
MP-97	<MDA	0.77
MP-98	<MDA	0.58
MP-100	8.5 ± 1.5	0.71

827

828

829 **Table 3.** Radiocarbon dating of MPG samples indicating their origin, the radiocarbon
830 age (^{14}C age BP) and the calibrated date using INTCAL13 curve and presented in
831 calendar years Common Era (CE). Samples in **red** and *italics* were not included in the
832 age model (see column “comments” and text for explanation).

Sample origin	Sample ID	Laboratory ID	^{14}C age BP	Cal age (CE)	Comments
Bulk organic matter	MP-1	D-AMS 025291	2000±64	8±66	Used in the age model
	MP-42	D-AMS 025294	1554±27	462±32	Used in the age model
	MP-48	D-AMS 025295	73±33	1897±20	Discarded due to plastic contamination
	MP-67	D-AMS 025296	876±29	1185±31	Used in the age model
	MP-68	D-AMS 026592	1128±22	942±24	Used in the age model
	MP-69	D-AMS 026593	1230±23	730±14	Used in the age model
	MP-70	D-AMS 025297	1308±28	680±16	Used in the age model
	MP-73	D-AMS 025298	1011±25	1012±16	Used in the age model
	MP-100	D-AMS 025299	923±39	1074±31	Used in the age model
Bulk material (filter)	MP-67filter	D-AMS 029894	485±40	1429±15	Discarded due to mixing with detrital fraction
	MP-81filter	D-AMS 033972	1758±25	287±68	
WIOC	MP10m	MP10m	812±755	854±721	Discarded due to too high error
	MP59m	MP59m	926±268	1046±242	Used in the age model
Pollen concentration	MP-30pollen	D-AMS 031464	3906±42	-2384±1332	Discarded due to technical issues and too high errors
	MP-70pollen	D-AMS 031465	1787±37	237±255	
	MP-100pollen	D-AMS 031466	1854±30	158±807	

833

834 **Table 4.** Elemental concentration (ppm) of major and trace metals in both Ordesa's
835 current deposited dust and MPG ice deposits (averaged values for the 35 analyzed
836 samples), as well as Upper Crust (UC) elemental contents for comparison (Taylor and
837 McLennan, 1995). On the right side, Al-normalised Enrichment Factors (EF) for dust
838 components and elements for: EF_i, the MPG ice dust versus the current Ordesa's
839 deposited dust (Codd); EF_{icodd}, the Codd versus the UC; and EF_{impgid}, the MPG ice
840 dust versus the UC. Numbers in bold type in the EF represent anomalous values
841 (elements enriched in Ordesa samples or in MPG ones).

	Ordesa 2016-2017 (2-year atmospheric deposition)			Monte Perdido (ice dust: 35 filter samples)			Upper Crust (ppm)	Al-Normalised Enrichment Factors		
	Max	Min (ppm)	Average	Max	Min (ppm)	Average		EF _i	EF _{icodd}	EF _{impgid}
OC	443270	49659	206814	436343	14793	126381		0,4		
EC	114519	12506	39995	112769	14668	40605		0,6		
Al	122401	7883	60410	506467	19611	98808	80400	1,0	1,0	1,0
Ca	22578	3182	9663	119648	256,7	11984	30000	0,8	0,4	0,3
Fe	63218	2901	32665	183957	12504	59477	35000	1,1	1,2	1,4
K	27478	3907	14839	57038	4001	18505	28000	0,8	0,7	0,5
Mg	27286	2105	12265	72210	3513	16645	13300	0,8	1,2	1,0
Na	5380	1,2	1413	25750	593	5126	28900	2,2	0,1	0,1
Ti	5035	257	2334	52192	3243	13662	3000	3,6	1,0	3,7
Mn	1656	128	582	3835	174	979	600	1,0	1,3	1,3
Sr	170	19	78	200	20	80	350	0,6	0,3	0,2
Be	7	0	2,1	2,3	0	0,4	3	0,1	0,9	0,1
V	208	10	76	257	28	107	60	0,9	1,7	1,5
Cr	720	5	118	2915	12	441	35	2,3	4,5	10,3
Co	32	0	7,6	49	5,4	20	10	1,6	1,0	1,6
Ni	414	7	55	1046	4,3	228	20	2,5	3,6	9,3
Cu	683	33	127	26451	92	3786	25	18,3	6,7	123,2
Zn	9391	164	1316	3826	171	988	71	0,5	24,7	11,3
As	26	2	10	51	5,3	18	1,5	1,0	9,1	9,6
Se	90	0	22	30	0	5,2	50	0,1	0,6	0,1
Cd	100	0	14	1,5	0	0,3	0,98	0,0	18,8	0,2
Sb	26	0	4,5	59	2	11	0,2	1,5	29,7	43,3
Ba	1010	15	287	870	67	317	550	0,7	0,7	0,5
Tl	1	0	0,1	1,1	0	0,2	0,75	1,7	0,1	0,2
Pb	175	8	53	2989	86	495	17	5,7	4,2	23,7
Th	37	1	12	26	1,6	9,7	10,7	0,5	1,5	0,7
U	8	0	2,5	15	0	3,7	2,8	0,9	1,2	1,1

842